doi.org/10.26434/chemrxiv.12052884.v1

Ligand Field-Actuated Non-Innocence of Acetylacetonate

Morten Gotthold Vinum, Laura Voigt, Steen Hansen, Colby Bell, Kensha Marie Clark, René Wugt Larsen, Kasper Pedersen

Submitted date: 31/03/2020 • Posted date: 01/04/2020

Citation information: Vinum, Morten Gotthold; Voigt, Laura; Hansen, Steen; Bell, Colby; Clark, Kensha Marie; Larsen, René Wugt; et al. (2020): Ligand Field-Actuated Non-Innocence of Acetylacetonate. ChemRxiv. Preprint. https://doi.org/10.26434/chemrxiv.12052884.v1

The quest for simple ligands to participate in concerted base metal-ligand multiple-electron redox events is driven by perspectives of replacing noble metals in catalysis and for discovering novel chemical reactivity. Yet the vast majority of simple ligand systems displays electrochemical potentials impractical for catalytic cycles substantiating the importance of new strategies towards aligned metal–ligand orbital energy levels. We herein demonstrate the possibility to establish and tame the elusive non-innocence of the ubiquitous acetylacetonate (acac), that is the most commonly employed anionic, chelating ligand towards elements across the entire Periodic Table. By employing the ligand field in the high-spin Cr(II) as a thermodynamic switch, we were able to chemically tailor the occurrence of metal–ligand redox events. The very mechanism can be understood as a destabilization of the d_z2 orbital relative to the pi* LUMO of acac, which proffers a generalizable strategy to synthetically engineer non-innocence with seemingly redox-inactive ligands.

Ligand field-actuated non-innocence of acetylacetonate†

Morten Gotthold Vinum,[a] Laura Voigt,[a] Steen H. Hansen,[a] Colby Bell,[b] Kensha Marie Clark,[b] René Wugt Larsen,[a] and Kasper S. Pedersen*,[a]

Received 00th January 20xx,
Accepted 00th January 20xx

DOI: 10.1039/x0xx00000x

The quest for simple ligands to participate in concerted base metal-ligand multiple-electron redox events is driven by perspectives of replacing noble metals in catalysis and for discovering novel chemical reactivity. Yet the vast majority of simple ligand systems displays electrochemical potentials impractical for catalytic cycles substantiating the importance of new strategies towards aligned metal–ligand orbital energy levels. We herein demonstrate the possibility to establish and tame the elusive *non-innocence* of the ubiquitous acetylacetonate (acac), that is the most commonly employed anionic, chelating ligand towards elements across the entire Periodic Table. By employing the ligand field in the high-spin Cr(II) as a thermodynamic switch, we were able to chemically tailor the occurrence of metal–ligand redox events. The very mechanism can be understood as a destabilization of the d_{z^2} orbital relative to the π^* LUMO of acac, which proffers a generalizable strategy to synthetically engineer non-innocence with seemingly redox-inactive ligands.

Introduction

Taming concerted metal ion-centered and ligand-centered redox processes paves the way for handling multi-electron redox events with base-metal ions, which challenge the role of the noble metals in catalysis.[1–5] Of particular interest are chelating ligands that both impose specific steric constraints and enhance the chemical robustness of the transition metal complex, whilst simultaneously serving as electron reservoirs that facilitate redox events at relatively mild electrochemical potentials.[6–9] A variety of bidentate ligands have been shown to exhibit beneficial redox-activity and cooperative metal-ligand reactivities. Overwhelmingly, this observed behavior is dominated by ligands that form five-membered chelate rings.[7,10] Six-membered chelate rings are largely dominated by β-diketonate ligands, the related β-enaminoketonate, and β-diketiminates,[11] which are ubiquitous in the chemistry of the s-, p-, d-, and f-block elements. Surprisingly, their redox-activity has remained largely unexplored, despite its potential for exploitation in homogeneous catalysis.[12,13] This lacuna arises from the high energy of the ligand LUMO of β-diketiminates, which requires the use of extremely strong reductants.[14] Consequently, they partake exclusively in ligand-centered oxidations.[14,15] Holland and co-workers demonstrated that the energy of the LUMO can be decreased significantly through the employment of the structurally related formazanate ligands, although strong reductants, as alkali metals, were still needed to induce ligand-centered reduction.[16–18] Quite surprisingly, the simple acetylacetonate ligand (acac = monoanion of pentane-2,4-dione) has never been reported to participate in redox events in transition metal chemistry. The existence of an unstable Li^+ and Mg^{2+}-bound anion radical, $acac^{\bullet 2-}$, generated by reduction with *n*-butyllithium or Grignard reagents, was suggested by EPR spectroscopy; however, the radical could not be isolated or studied in any further detail.[19]

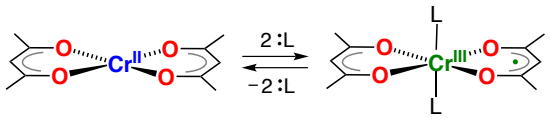

Scheme 1. Switching of the redox-state of acetylacetonate by axial coordination/de-coordination at a Cr(II)/Cr(III) center.

We recently demonstrated that six-coordinate *trans*-$[Cr(hfac)_2L_2]$ (hfac = 1,1,1,5,5,5-hexafluoroacetylacetonate; *L* = pyrazine, or tetrahydrofuran) is most adequately described as a Cr(III) complex with a single unpaired electron delocalized over two $hfac^-$ ligands.[20] In contrast, the related square-planar complex $[Cr(acac)_2]$, reported in 1958,[21] is known to possess an $S = 2$ spin ground state, which is indicative of a high-spin Cr(II) center.[21,22] Herein, we show that introduction of modest σ donors in the vacant, axial positions of $[Cr(acac)_2]$ leads to loss of

[a] *Department of Chemistry, Technical University of Denmark, Kemitorvet, DK-2800 Kgs. Lyngby, Denmark. E-mail: kastp@kemi.dtu.dk*
[b] *Department of Chemistry, The University of Memphis, Memphis, TN, USA.*

† Electronic Supplementary Information (ESI) available: Full experimental details, solution UV-vis spectroscopic data, crystallographic details, powder X-ray diffraction data, DFT-calculated frontier molecular orbitals. See DOI: 10.1039/x0xx00000x

innocence of the acac ligand (Scheme 1), providing a novel route to chemically control the electronic delocalization - and spin-density in a metal-ion complex.

Results and discussion

The crystallographic evidence for the existence of a chromium(II) acetylacetonate was reported by Cotton *et al.* in 1977.[22] Sublimation of crude [Cr(acac)$_2$] concomitantly yielded crystalline [Cr(acac)$_2$] and [Cr(acac)$_3$]. We found that reaction of stoichiometric amounts of Li(acac) and $CrCl_2$ in dry, deoxygenated tetrahydrofuran (THF) provides a convenient, direct route to crystalline, brown-orange [Cr(acac)$_2$] (**1**, see ESI for details). Our redetermination of the crystal structure of **1** at T = 120 K revealed only a minor thermal contraction as compared to the previously reported room temperature structure.[22] Notably, the Cr center resides in a square planar coordination environment that is distantly stacked into a supramolecular chain structure (Fig. 1) with presumably weak [Cr(acac)$_2$]···[Cr(acac)$_2$] interactions. Dissolution of **1** in a selection of weakly coordinating solvents, like THF, toluene, and acetonitrile, leads to only weakly colored solutions (Fig. S1, ESI†). The absorption bands above λ = 500 nm are of low intensity (ε < 200 M^{-1} cm^{-1}) and are identified as metal-centered d-d transitions. In pyridine, however, an intense, dark coloration of the solution occurs. The UV-vis spectrum (Fig. S1, ESI†) reveals strong optical absorption (ε = 800–13,000 M^{-1} cm^{-1}) through the entire spectral range (200–1000 nm) with onset of an intense charge-transfer band at ~700 nm. The cooling of concentrated pyridine solutions of **1** affords black crystalline specimens, which were identified as *trans*-[Cr(acac)$_2$(pyridine)$_2$] (**3**) by single-crystal X-ray diffraction. The average Cr—O bond length in **3** (1.94 Å) is significantly shorter than that of **1** (1.98 Å) despite the lower coordination number in **1**. Furthermore, the average C—O bond length is elongated from 1.27 Å in **1** to 1.29 Å in **3** (Fig. 2). This minimalistic structural analysis could suggest an evolution in the electronic structure, bounded by {Cr^{II}–(acac)$_2^{2-}$} in **1** and {Cr^{III}–(acac)$_2^{\bullet 3-}$} in **3**, as the extreme, limiting cases. The formulation of {Cr^{III}–(acac)$_2^{\bullet 3-}$} implies a concurrent occupation of the antibonding LUMO of the acac ligands, which, is expected to predominantly elongate the C—O bonds.[20] To corroborate this hypothesis, two additional [Cr(acac)$_2L_2$] complexes with the axial ligands containing an electron-poor (L = 4-(trifluoromethyl)pyridine = CF_3py; **2**) and an electron-rich (L = 4-(dimethylamino)pyridine = DMAP; **4**) pyridine ring were synthesized and structurally characterized (Fig. 1). The average Cr—N and Cr—O bond lengths in **2**–**4** vary only slightly (≤0.6%) indicating a common oxidation state of the Cr center. The differences within the series become clearer with the metrics of the acac ligand. Whereas **1** stands apart with the shortest averaged C—O bond of 1.271 Å, the C—O bond elongates by 2.4% from **1**, over **2** and **3**, to **4** (and by 1.2% from **2** to **4**; Fig. 2). Herein, the C—O bond of **4** is within the longest 3% of the averaged C—O bond lengths of all reported acac-based structures (Fig. 2). On the contrary, the C—CH and C—CH_3 bond lengths are identical within the experimental accuracy across the entire series **1**–**4**. Cyclic voltammetry of **1** in pyridine, presumably forming solvated **3**, affords a single reversible oxidation at $E_{1/2}$ = –1.17 V vs Cp*$_2$Fe$^{0/+}$, assigned to the formation of *trans*-[Cr^{III}(acac)$_2$(pyridine)$_2$]$^+$ (**3**$^+$, Fig. S4, ESI†).

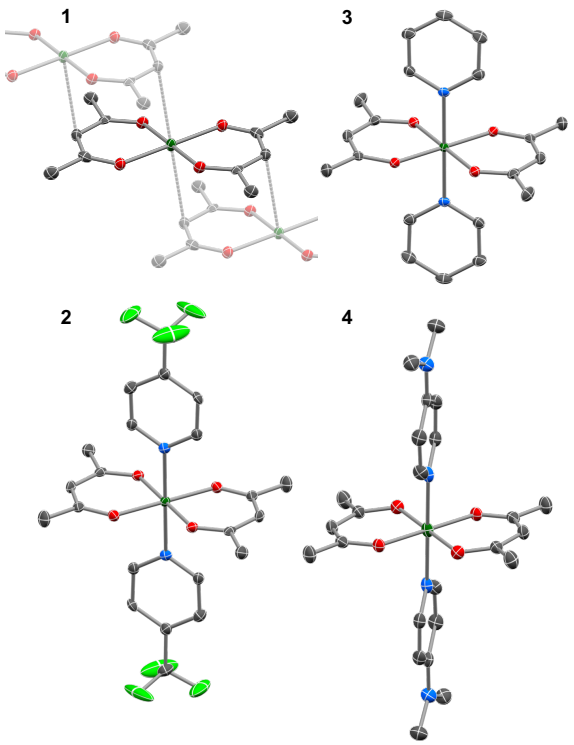

Fig. 1. Thermal ellipsoid plots of the single-crystal X-ray (T = 120(1) K) structures of **1**–**4** shown at 50% probability level. Hydrogen atoms have been omitted for clarity. Color code: Cr, dark green; F, pale green; O, red; N, blue, C, grey. Selected bond lengths (Å): **1** ($P2_1/n$): Cr—O 1.983(3), 1.984(3), C—O 1.271(5), 1.272(5), Cr···Cγ 2.997; **2** ($P2_1/c$): Cr—O 1.952(3), 1.958(2), Cr—N 2.072(3), C—O 1.282(4), 1.292(5); **3** ($P2_1/n$): Cr—O 1.938(2), 1.947(2), Cr—N 2.085(2), C—O 1.292(3), 1.294(3); **4** ($P\bar{1}$): Cr—O 1.947(2), 1.949(2), Cr—N 2.096(3), C—O 1.299(4), 1.305(4).

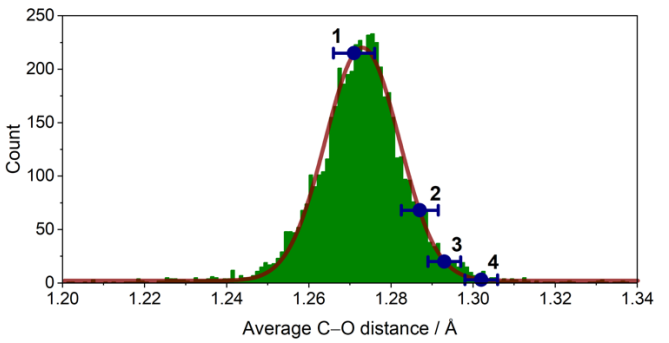

Fig. 2. Histogram of the average C—O distance in *all* crystallographically characterized acac complexes deposited in the Cambridge Structural Database (~3000) with indicated average bond lengths for **1**–**4**. The solid, red line is a Gaussian fit with μ = 1.2731 Å, σ = 0.0180 Å.

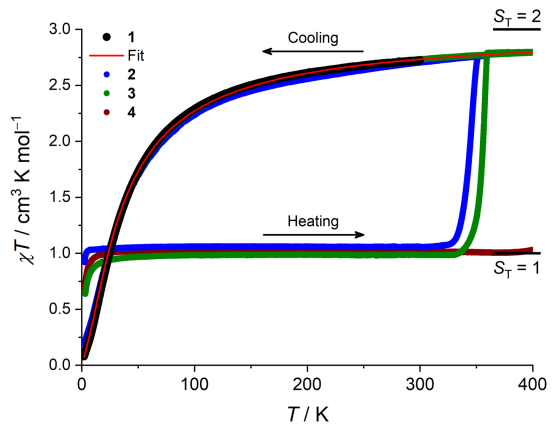

Fig. 3. Temperature dependence of the magnetic susceptibility-temperature, χT, product obtained with a magnetic field of $\mu_0 H$ = 1.0 T ($\Delta T/\Delta t$ = 1 K min^{-1} for 2–300 K, and 0.1 K min^{-1} for 300–400 K). The red line is the best fit to the classical Fisher model as described in the main text. The short vertical lines indicate the calculated Curie limits for S_T = 1 and S_T = 2 with a g-factor of 2.0.

3$^+$ has previously been isolated as the PF_6^- salt and the RT crystal structure exhibits a slightly longer Cr—O bond length (1.950(2) Å) and a slightly shorter C—O bond length (1.289(2) Å) than those found in **3**, supporting the presence of a partially reduced acac-ligand scaffold in **3**.[23] Notably, dichloromethane solutions of **3** display irreversible oxidation waves suggesting a dynamic ligand exchange.

Whilst being known to exhibit a S = 2 ground state at room temperature,[21] the magnetic properties of **1** have not previously been studied in any further detail. The room temperature value of the susceptibility-temperature, χT, product for **1** (Fig. 3, black trace) amounts to 2.7 cm^3 K mol^{-1}, which is slightly lower than the expected value (3.0 cm^3 K mol^{-1}) for a magnetically uncoupled S = 2 ion with a g-factor of 2.0. Upon decreasing temperature, the χT product decreases
and almost vanishes at 2 K. The crystal structure of **1** features supramolecular $[Cr(acac)_2]_\infty$ chains running along the crystallographic b direction with intermolecular distances of Cr···Cr = 4.7 Å and Cr···Cγ = 3.0 Å (Fig. 1), which provides a pathway for weak intermolecular superexchange interactions. The χT vs T data can be modelled by the classical Fisher model for S = 2 chains using the isotropic Hamiltonian:[24]

$$\widehat{\mathcal{H}} = J\sum_{1}^{N}\hat{S}_i\hat{S}_{i+1} + g\mu_B\mu_0 H\sum_{1}^{N}\hat{S}_i$$

Here the summation runs from the first spin center to the Nth spin center and the symbols have their usual meaning. The strength of the intrachain superexchange interaction is parametrized by J. The best-fit to the experimental data afforded J = 7.0(1) cm^{-1} and g = 2.0(1) (Figs 3, S5, ESI†). Assuming that the dominant interaction is along the chain-direction, broken-symmetry (BS) DFT calculations, at the TPSSh/def2-TZVP-ZORA level, on a dimeric $\{Cr^{II}(acac)_2\}_2$ chain fragment provides J = 6.4 cm^{-1}, in good agreement with the experimentally determined value of J (see ESI† for further details). The field dependence of the magnetization, M vs H, at selected temperatures between 2 and 16 K is close to linear (Fig. S6, ESI†). This observation is coherent with the presence of a non-magnetic ground state inferred by the sizable intrachain antiferromagnetic interactions. In contrast to **1**, the room temperature χT products for **2**–**4** are all close to 1.0 cm^3 K mol^{-1} reflecting an S_T = 1 ground state (Fig. 3; **2**: 1.05 cm^3 K mol^{-1}, **3**: 0.99 cm^3 K mol^{-1}, **4**: 1.02 cm^3 K mol^{-1}). The S_T = 1 may be obtained in low-spin Cr(II) complexes, which, however, are rare and *only* found together with ligands placed in the extreme end of the spectrochemical series (CN^-, CO, phosphines, etc.).[25,26] Alternatively, an S_T = 1 ground state may arise from the antiferromagnetic interaction between a radical spin and a S = 3/2 Cr(III).[25] If the superexchange coupling constant between these two spin-bearing units is on the order of the thermal energy at room temperature, or larger, the χT product reflects an energetically isolated S_T = 1 state in the full experimental temperature window. Indeed, the χT products of **2**–**4** remain constant on descending temperature before experiencing a decline at the lowest temperatures, which can be attributed to concerted effects of weak intermolecular superexchange interactions and magnetic anisotropy. The low-temperature magnetization vs field, M vs $\mu_0 H$, data for **2**–**4** (Fig. S6, ESI†) were fitted to the spin-Hamiltonian pertaining to tetragonal symmetry and acting on the S_T = 1 state:

$$\widehat{\mathcal{H}} = g\mu_B\mu_0\,\mathbf{H}\cdot\hat{\mathbf{S}}_T + D\left(\hat{S}_{T,z}^2 - S_T(S_T+1)/3\right)$$

The data could be modelled with the D/hc parameters of +2.2 cm^{-1}, +4.2 cm^{-1}, and +3.7 cm^{-1} for **2**, **3**, and **4**, respectively. These values are large for Cr(III) complexes ($D_{Cr(III)} = 2/3 \times D$), although not unprecedented.[27] Heating **2**–**4** above room temperature (0.1 K min^{-1}) leads to abrupt increases in the χT products at ~330 K and ~340 K for **2** and **3**, respectively, which saturate at ~2.8 cm^3 K mol^{-1} at ~350 K (**2**) and ~360 K (**3**). Notably, the χT product of **4** experiences only a minuscule increase at the highest reachable temperature (400 K). Powder X-ray diffraction identifies the heated samples of both **2** and **3** as phase-pure, microcrystalline **1** (Fig. S3, ESI†). The subsequent re-cooling to 2 K demonstrates the irreversibility of the thermal cycling (Fig. 3) where the χT product decreases monotonically to 0.08 cm^3 K mol^{-1} at 2 K, identical to the data obtained for as-synthesized **1** (Fig. 3, black trace).

Solid state attenuated total reflection spectra in the infrared spectral range echo the electronic structure conclusions as acquired from crystallography and magnetometry (Fig. 4). For **1**, the near-infrared (NIR) region is void of absorptions and the only identifiable, narrow bands fall in the mid-IR region where they are assigned as being of vibrational origin. For **2**–**4**, an intense, broad absorption is observed at ~8800 cm^{-1} for **2**

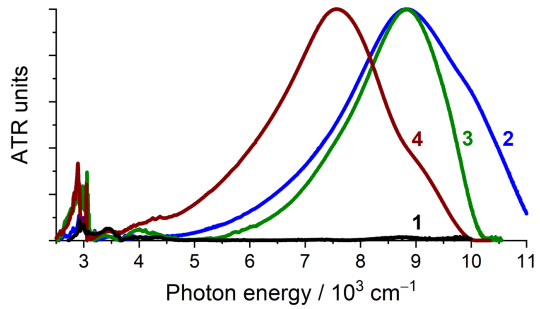

Fig. 4. Room temperature attenuated total reflectance (ATR) IR spectra of polycrystalline **1**–**4**. The spectra were normalized to unity at the absorption maximum, except for the spectrum of **1**, which was scaled by superposing the vibrational bands to those of **2**.

and **3**, and at ~7600 cm^{-1} for **4**. The spectral maxima of the near-IR spectra of **2** and **3** virtually coincide, but the band width is significantly different. Intense NIR excitations are commonly considered as fingerprints of mixed-valency and interpreted as inter-valence charge transfer transitions (IVCTs).[28,29] On the contrary, a complete absence of any absorption bands in the NIR energy window in **1** supports the {Cr^{II}–$(acac)_2^{2-}$} formulation.

Further insight into the electronic structures of **1**–**4** was acquired through DFT calculations performed on the experimentally determined molecular structures, without any subsequent geometry optimization, and at the TPSSh/def2-TZVP-ZORA level. For **1**, the high-spin (HS), S = 2, state is strongly stabilized over the S_T = 1 (3,1)-broken-symmetry state (BS; the notation referring to a state with 3 unpaired α-spins on one fragment and 1 unpaired β-spin on a different fragment) ($E_{HS} - E_{BS}$ = –9518 cm^{-1}) in accordance with the preceding experimental results. The Mulliken spin population of the Cr center in **1** (Fig. 5) amounts to 4.1, consistent with the presence of a HS Cr(II) ion. Furthermore, the summed Mulliken spin population for each acac ligand vanishes at –0.05, as expected for a closed-shell ligand. The Kohn-Sham singly occupied molecular orbitals (SOMOs, Fig. S7, ESI†) are all of predominant 3d-character suggesting little admixture with ligand-based π-orbitals. These observations contrast starkly the situation for **2**–**4**, where the (3,1)-BS states are strongly stabilized relative to the HS states (**2**: 7248 cm^{-1}; **3**: 8078 cm^{-1}; **4**: 5656 cm^{-1}), suggesting a ground state formulated as {Cr^{III}–$(acac)_2^{\bullet 3-}$}. Using a superexchange Hamiltonian of the form $\widehat{\mathcal{H}} = J\,\widehat{S}_{Cr}\widehat{S}_{radical}$ (see ESI† for further details), the calculated energy gaps are translated into superexchange coupling constants, J, of 3943 cm^{-1}, 4366 cm^{-1}, and 3114 cm^{-1} for **2**, **3**, and **4**, respectively. Whilst the irregular evolution is not straightforward to explain, the magnitudes reflect extremely strong antiferromagnetic interactions, which are approximately one order of magnitude larger than the values estimated experimentally or calculated for other Cr(III)-radical complexes.[25,26,30–33] The Mulliken spin-populations of Cr amounts to 2.7 for all three members of the series, **2**–**4**. This value is close to the expected values for an S = 3/2 ion of 3.0 (Fig. 5), and of similar magnitude as several other established Cr(III) complexes with redox-active ligands.[25] Despite the close resemblance in the Cr spin density for **2**–**4**, a clear evolution of the Mulliken spin population of the acac ligands and the axial pyridine ligands is observed (Fig. 5). The summed spin density per acac ligand in **2** amounts to 0.2, which is significantly larger than found for **1**. For **3**, only a slight increase in the acac spin density relative to **2** is found, whereas the integrated acac spin population in **4** of 0.4 approaches the expectation for one electron fully delocalized over two acac moieties (0.5). The evolution of the axial pyridines' spin density counter-balances that of the acac ligand, i.e. showing a gradual decrease in the spin density from a sizable value in **2** of –0.3 to a vanishing value in **4** (–0.06). This trend follows the anticipated one based on the electron density of the pyridines. Noticeably, as opposed to **1**, for all members of **2**–**4**, the highest energy SOMO is of predominant ligand p-orbital character, whereas the three energetically lower-lying, quasi-degenerate SOMOs all are metal-based and reminiscent of the d_{xy}, d_{yz}, and d_{zx} orbitals (Figs. S8-10, ESI†).

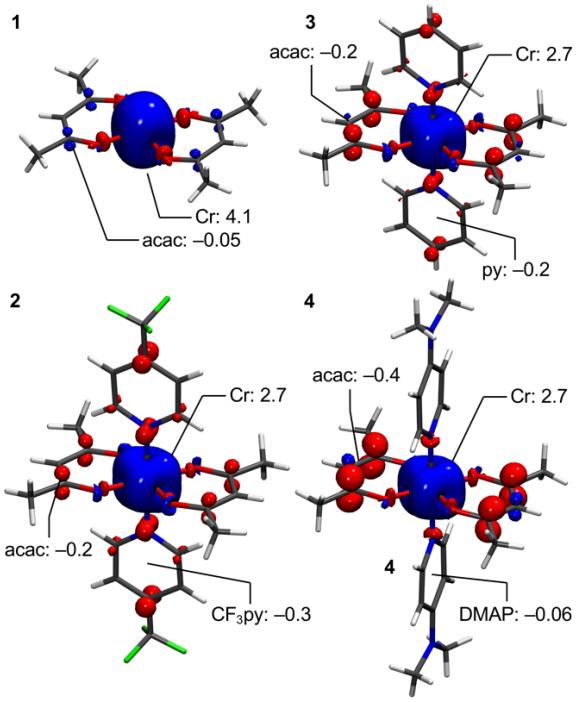

Fig. 5. DFT-calculated spin-density plots of the HS-state of **1** and the BS-states of **2**–**4** shown at an isosurface value of 0.005 a.u. Selected Mulliken spin populations are indicated.

Conclusion

We have demonstrated the redox-noninnocence of the ubiquitous acetylacetonate ligand. The crystallographic, magnetic, spectroscopic, and computational results all point toward the occurrence of concerted metal-ligand redox chemistry in the square-planar [$Cr(acac)_2$] upon axial coordination of strongly donating pyridine ligands. In

the ideally square-planar ligand field of **1**, the singly occupied d_{z^2} orbital remains energetically low-lying, whereas, as previously hypothesized,[20] the pyridines of **2**–**4** raise the d_{z^2} orbital above the ligand-based LUMO, leading to a partial $\{Cr^{II}–(acac)_2^{2-}\} \rightarrow \{Cr^{III}–(acac)_2^{\bullet 3-}\}$ valence tautomerization. The presence of both a single crystallographically unique acac and pyridine-type ligand in each of **2**–**4** suggests delocalization of the radical spin via the Cr center (in contrast to the simplified drawing in Scheme 1). Thus, **2**–**4** may be assigned as ligand-based class II/III mixed-valency systems according to the Robin-Day classification.[28] Notably, the valence tautomerization in $[Cr(acac)_2]$ is not triggered by more weakly coordinating ligands, which may leave the d_{z^2} orbital energetically well below the ligand acac LUMO. Displacement of the pyridine ligands in **2**–**4** demonstrates the reversibility of the $\{Cr^{II}–(acac)_2^{2-}\} \rightleftarrows \{Cr^{III}–(acac)_2^{\bullet 3-}\}$ valence tautomerization process. A handful of transition metal complex families demonstrate temperature-induced valence tautomerism,[34,35] but the manifestation of ligand noninnocence upon alteration of the metal ligand sphere is exceedingly rare.[36] The valence tautomers **2**–**4** exhibit extremely strong Cr(III)-radical exchange interactions, as demonstrated by magnetization measurements and DFT calculations. The importance of exceedingly strong metal-ligand exchange interactions was recently highlighted as key for acquiring efficient electrocatalysis,[37] although the tailoring of superexchange has so far received limited attention in catalysis. Apart from the presented chemical triggering of the valence tautomerization, it is tempting to speculate if mechanical stimuli, mimicking an increased axial ligand field, may actuate noninnocence in **1**. Quite notably, **1** is isomorphous to $[Cu(acac)_2]$, which has recently been shown to form easily deformable crystals.[38–40] Any similar plasticity in crystals of **1** could hence be coupled to dramatic changes in both the optical and magnetic properties following the $\{Cr^{II}–(acac)_2^{2-}\} \rightleftarrows \{Cr^{III}–(acac)_2^{\bullet 3-}\}$ valence tautomerization.

Conflicts of interest

There are no conflicts to declare.

Acknowledgements

K.S.P. thanks the VILLUM Foundation for a VILLUM Young Investigator grant (15374), and the Carlsberg Foundation (CF-17-0637), the Brdr. Hartmann's Foundation and the Torkil Holm foundation for research infrastructure grants.

Notes and references

‡ Footnotes relating to the main text should appear here. These might include comments relevant to but not central to the matter under discussion, limited experimental and spectral data, and crystallographic data.

1 D. L. J. Broere, R. Plessius and J. I. Van Der Vlugt, *Chem. Soc. Rev.*, 2015, **44**, 6886–6915.
2 V. K. K. Praneeth, M. R. Ringenberg and T. R. Ward, *Angew. Chem. Int. Ed.*, 2012, **51**, 10228–10234.
3 P. J. Chirik and K. Wieghardt, *Science*, 2010, **327**, 794–795.
4 O. R. Luca and R. H. Crabtree, *Chem. Soc. Rev.*, 2013, **42**, 1440–1459.
5 V. Lyaskovskyy and B. De Bruin, *ACS Catal.*, 2012, **2**, 270–279.
6 W. Kaim and B. Schwederski, *Coord. Chem. Rev.*, 2010, **254**, 1580–1588.
7 W. Kaim, *Dalton Trans.*, 2019, **48**, 8521–8529.
8 S. Ganguly and A. Ghosh, *Acc. Chem. Res.*, 2019, **52**, 2003–2014.
9 R. Eisenberg and H. B. Gray, *Inorg. Chem.*, 2011, **50**, 9741–9751.
10 M. M. Khusniyarov, T. Weyhermüller, E. Bill and K. Wieghardt, *J. Am. Chem. Soc.*, 2009, **131**, 1208–1221.
11 L. Bourget-Merle, M. F. Lappert and J. R. Severn, *Chem. Rev.*, 2002, **102**, 3031–3065.
12 C. Camp and J. Arnold, *Dalton Trans.*, 2016, **45**, 14462–14498.
13 R. L. Webster, *Dalton Trans.*, 2017, **46**, 4483–4498.
14 M. M. Khusniyarov, E. Bill, T. Weyhermüller, E. Bothe and K. Wieghardt, *Angew. Chem. Int. Ed.*, 2011, **50**, 1652–1655.
15 M. P. Marshak, M. B. Chambers and D. G. Nocera, *Inorg. Chem.*, 2012, **51**, 11190–11197.
16 D. L. J. Broere, B. Q. Mercado, J. T. Lukens, A. C. Vilbert, G. Banerjee, H. M. C. Lant, S. H. Lee, E. Bill, S. Sproules, K. M. Lancaster and P. L. Holland, *Chem. Eur. J.*, 2018, **24**, 9417–9425.
17 D. L. J. Broere, B. Q. Mercado, E. Bill, K. M. Lancaster, S. Sproules and P. L. Holland, *Inorg. Chem.*, 2018, **57**, 9580–9591.
18 M. C. Chang, P. Roewen, R. Travieso-Puente, M. Lutz and E. Otten, *Inorg. Chem.*, 2015, **54**, 379–388.
19 A. Staško, A. Tkáč, V. Laurinc and L. Malík, *Org. Magn. Reson.*, 1976, **8**, 237–239.
20 M. G. Vinum, L. Voigt, C. Bell, D. Mihrin, R. W. Larsen, K. M. Clark and K. S. Pedersen, *Chem. Eur. J.*, 2020, **26**, 2143–2147.
21 G. Costa and A. Puxeddu, *J. Inorg. Nucl. Chem.*, 1958, **8**, 104–112.
22 F. A. Cotton, C. E. Rice and G. W. Rice, *Inorg. Chim. Acta*, 1977, **24**, 231–234.
23 A. Iino, T. Suzuki and S. Kaizaki, *J. Chem. Soc. Dalton Trans.*, 2003, **3**, 4604–4611.
24 M. E. Fisher, *Am. J. Phys.*, 1964, **32**, 343–346.
25 C. C. Scarborough, S. Sproules, C. J. Doonan, K. S. Hagen, T. Weyhermüller and K. Wieghardt, *Inorg. Chem.*, 2012, **51**, 6969–6982.
26 C. C. Scarborough, S. Sproules, T. Weyhermüller, S.

DeBeer and K. Wieghardt, *Inorg. Chem.*, 2011, **50**, 12446–12462.
27 J. Krzystek, G. Kohl, H. B. Hansen, M. Enders and J. Telser, *Organometallics*, 2019, **38**, 2179–2188.
28 M. B. Robin and P. Day, *Adv. Inorg. Chem. Radiochem.*, 1968, **10**, 247–422.
29 D. M. D'Alessandro and F. R. Keene, *Chem. Soc. Rev.*, 2006, **35**, 424–440.
30 M. Wang, J. England, T. Weyhermüller, S. L. Kokatam, C. J. Pollock, S. DeBeer, J. Shen, G. P. A. Yap, K. H. Theopold and K. Wieghardt, *Inorg. Chem.*, 2013, **52**, 4472–4487.
31 J. A. DeGayner, I. R. Jeon and T. D. Harris, *Chem. Sci.*, 2015, **6**, 6639–6648.
32 C. Hua, J. A. DeGayner and T. D. Harris, *Inorg. Chem.*, 2019, **58**, 7044–7053.
33 X. Ma, E. Suturina, M. Rouzieres, F. Wilhelm, A. Rogalev, R. Clérac and P. Dechambenoit, *Chem. Commun.*, 2020, DOI: 10.1039/D0CC00548G.
34 D. N. Hendrickson and C. G. Pierpont, in *Spin Crossover in Transition Metal Compounds II*, Springer Berlin Heidelberg, Berlin, Heidelberg, 2004, pp. 63–95.
35 J. Bendix and K. M. Clark, *Angew. Chem.*, 2016, **128**, 2798–2802.
36 E. J. Schelter, R. Wu, B. L. Scott, J. D. Thompson, T. Cantat, K. D. John, E. R. Batista, D. E. Morris and J. L. Kiplinger, *Inorg. Chem.*, 2010, **49**, 924–933.
37 J. S. Derrick, M. Loipersberger, D. A. Iovan, P. T. Smith, K. Chakarawet, J. R. Long, M. Head-Gordon and C. J. Chang, *ChemRXiv*, 2020, DOI:10.26434/chemrxiv.11923176.v1.
38 A. Worthy, A. Grosjean, M. C. Pfrunder, Y. Xu, C. Yan, G. Edwards, J. K. Clegg and J. C. McMurtrie, *Nat. Chem.*, 2018, **10**, 65–69.
39 A. J. Brock, J. J. Whittaker, J. A. Powell, M. C. Pfrunder, A. Grosjean, S. Parsons, J. C. McMurtrie and J. K. Clegg, *Angew. Chem. Int. Ed.*, 2018, **57**, 11325–11328.
40 E. P. Kenny, A. C. Jacko and B. J. Powell, *Angew. Chem. Int. Ed.*, 2019, **58**, 15082–15088.

Ligand field-actuated non-innocence of acetylacetonate

Morten Gotthold Vinum,[1] Laura Voigt,[1] Steen H. Hansen,[1] Colby Bell,[2] Kensha M. Clark,[2] René Wugt Larsen,[1] and Kasper S. Pedersen[1]

[1] Department of Chemistry, Technical University of Denmark, DK-2800 Kgs. Lyngby, Denmark

[2] Department of Chemistry, The University of Memphis, Memphis, TN, USA

Synthesis

All reactions and manipulations were carried out under strictly anaerobic conditions in an inert Ar atmosphere using an InertLab glovebox operating with < 0.5 ppm O_2 and H_2O. Reagents were used as received. Dry and air-free solvents were supplied by a Puresolv MD 7 solvent purifications system. acacH = 2,4-pentanedione; py = pyridine; DMAP = 4-(dimethylamino)pyridine; CF_3py = 4-(trifluoromethyl)pyridine.

*Synthesis of $Cr(acac)_2$ (**1**)*

In a beaker, $CrCl_2$ (367 mg, 3.0 mmol) was suspended in dry THF (20 mL) and Li(acac) (630 mg, 5.95 mmol) was added under stirring. The mixture slowly turned dark and the reaction proceeded to completion over a 24-hour period. An orange single-crystalline precipitate of the desired compound separated out and was filtered off, washed with diethyl ether (2 × 10 mL) and dried on a glass frit. Yield: 524 mg (70% based on Cr). Crystals suitable for X-ray analysis could be isolated directly from the product. Elemental analysis calculated (found) for $C_{10}H_{14}CrO_4$ (%): C: 48.00 (47.68), H: 5.64 (6.12).

*Synthesis of $Cr(acac)_2(CF_3py)_2$ (**2**)*

To a suspension of **1** (50 mg, 0.2 mmol) in toluene (2 mL) was added 4-trifluoromethylpyridine (0.10 mL, 0.86 mmol). The solution instantaneously changed color to black and a precipitate of **2** started forming within minutes. The mixture was allowed to stand for 1 hour to ensure complete precipitation. Yield: 78 mg (72% based on **1**). Crystals suitable for X-ray analysis could be isolated directly from the product. Elemental analysis calculated (found) for $C_{22}H_{22}N_2O_4F_6Cr$ (%): C: 48.54 (47.11), H: 4.07 (4.13), N: 5.15 (4.82).

*Synthesis of $Cr(acac)_2(py)_2$ (**3**)*

To a suspension of **1** (108 mg, 0.43 mmol) in acetonitrile (2 mL) was added pyridine (2 mL) and the mixture immediately changed color to a very dark green. The mixture was left at room temperature for 24 hours to ensure complete precipitation of **3**. Yield: 120 mg (68% based on **1**). Crystals suitable for X-ray analysis could be isolated directly from the product. Elemental analysis calculated (found) for $C_{20}H_{24}CrN_2O_4$ (%): C: 58.82 (58.73), H: 5.92 (6.02), N: 6.86 (6.78).

*Synthesis of $Cr(acac)_2(DMAP)_2$ (**4**)*

To a suspension of **1** (135 mg, 0.54 mmol) in acetonitrile (5 mL) was added a solution of 4-(dimethylamino)pyridine (205 mg, 1.68 mmol) dissolved in acetonitrile (2.5 mL). The solution immediately changed color to black and the precipitation of **4** could be observed within minutes. The solution was allowed to stand for 24 hours to ensure complete crystallization. Yield: 195 mg (73% based on **1**). Crystals suitable for X-ray analysis could be isolated directly from the product.

Elemental analysis calculated (found) for $C_{24}H_{34}CrN_4O_4$ (%): C: 58.29 (58.16), H: 6.93 (7.02), N: 11.33 (11.09).

Spectroscopy

Solution ultraviolet-visible range absorption spectra of **1** in various solvents were acquired using a Cary 5 spectrophotometer and are compiled in Fig. S1. The spectra have all been corrected for instrumental and solvent background. The attenuated-total-reflectance (ATR) NIR spectra of solid, polycrystalline samples of **1**-**4**, presented in the main text (Fig. 4), were collected using a Bruker VERTEX80v Fourier Transform vacuum spectrometer employing a single-reflection diamond ATR module. The apparatus was configured with a CaF_2 beam splitter, a liquid nitrogen cooled InSb detector and a NIR tungsten radiation source. The collected ATR spectra of 4 cm^{-1} resolution have been corrected for residual water vapor absorption and the resulting spectra have been corrected for minor baseline drifts. Subsequently, extended ATR corrections were applied to account for the wavelength-dependent penetration depth of the NIR probe beam.

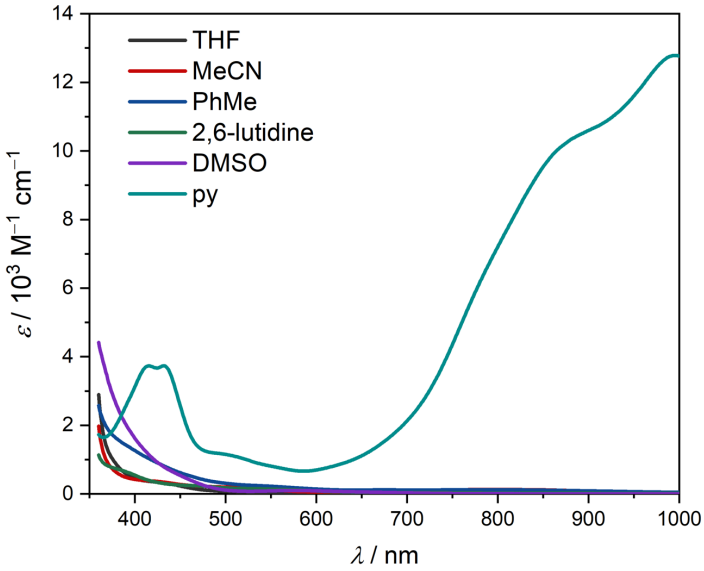

Figure S1. Solution UV-vis spectra of **1** dissolved in different, indicated solvents. The concentration of **1** in each solvent was: MeCN: 1.33×10^{-4} M, PhMe: 1.34×10^{-4} M, THF: 1.30×10^{-4} M, py: 1.29×10^{-4} M, 2,6-lutidine: 1.37×10^{-4} M, DMSO: 1.37×10^{-4} M.

Crystallography

Single crystals of **1**–**4** were sealed under a dry argon atmosphere using polybutene oil (Aldrich, >90%) before being exposed to ambient conditions. With a nylon loop, suitable crystals were selected under a microscope and mounted on a SuperNova Dual Source CCD-diffractometer. The crystal was kept at a constant temperature during data collection. Using Olex2,[1] the structure was solved using Charge Flipping using the olex.solve.structure solution program of Olex2 and refined by Least Squares using version 2014/7 of ShelXL.[2] All non-hydrogen atoms were refined anisotropically. Hydrogen atom positions were calculated geometrically and refined using the riding model.

The PXRD patterns of **1**-**4** were measured in sealed tape pockets (free of sharp Bragg-like peaks) in transmission with a Huber G670 powder diffractometer using Cu Kα1 (λ = 1.5406 Å, quartz monochromator) radiation. Samples measured after a PPMS experiment were first introduced back into an inert atmosphere, before being freed from the measurement capsule and subsequently sealed in a tape pocket.

Table 1. Crystallographic information and refinement parameters for **1–4**.

Compound	**1**	**2**	**3**	**4**
CCDC number	1974983	1974982	1974980	1974981
Empirical formula	$C_{10}H_{14}CrO_4$	$C_{22}H_{22}N_2O_4F_6Cr$	$C_{20}H_{24}CrN_2O_4$	$C_{24}H_{34}CrN_4O_4$
Formula weight / g mol^{-1}	250.21	544.41	408.41	494.55
Temperature / K	120.00	120	120	120.00
Crystal system	monoclinic	monoclinic	monoclinic	triclinic
Space group	$P2_1/n$	$P2_1/c$	$P2_1/n$	$P\bar{1}$
a / Å	10.2476(13)	9.9399(10)	9.8861(8)	7.9894(7)
b / Å	4.7011(6)	9.5252(9)	7.5065(8)	8.5405(8)
c / Å	11.3501(15)	12.1430(10)	12.9438(10)	9.4779(9)
α / °	90	90	90	103.054(8)
β / °	92.163(12)	94.290(8)	94.152(7)	101.710(8)
γ / °	90	90	90	92.188(7)
Volume / Å^3	546.40(12)	1146.47(18)	958.04(14)	614.49(10)
Z	2	2	2	1
ρ_{calc} / g cm^{-3}	1.521	1.577	1.416	1.336
μ / mm^{-1}	1.037	0.580	0.625	0.502
F(000)	260.0	556.0	428.0	262.0
Radiation	Mo Kα (λ = 0.71073)	Mo Kα (λ = 0.71073)	Mo Kα (λ = 0.71073)	Mo Kα (λ = 0.71073)
θ range for data collection / °	7.2–52.7	6.7–54.2	6.3–54.2	6.9–52.7
Index ranges	$-12 \le h \le 12$	$-9 \le h \le 12$	$-10 \le h \le 12$	$-9 \le h \le 8$
	$-5 \le k \le 4$	$-12 \le k \le 12$	$-9 \le k \le 6$	$-10 \le k \le 8$
	$-10 \le l \le 14$	$-15 \le l \le 15$	$-14 \le l \le 16$	$-11 \le l \le 11$
Reflections collected	2302	5379	4889	5094
Independent reflections	1114 [R_{int} = 0.0636]	2477 [R_{int} = 0.0492]	2086 [R_{int} = 0.0514]	2494 [R_{int} = 0.0526]
Data/restraints/parameters	1114/0/72	2477/0/162	2086/0/126	2494/0/155
Goodness-of-fit on F^2	1.073	1.046	1.034	1.091
Final R_1 index [$F^2 \ge 2\sigma(F^2)$]	0.062	0.063	0.0488,	0.060
Final wR_2 index [F^2]	0.095	0.126	0.0895	0.105
Largest diff. peak/hole / e Å^{-3}	0.54/–0.51	0.74/–0.55	0.45/–0.47	0.35/–0.39

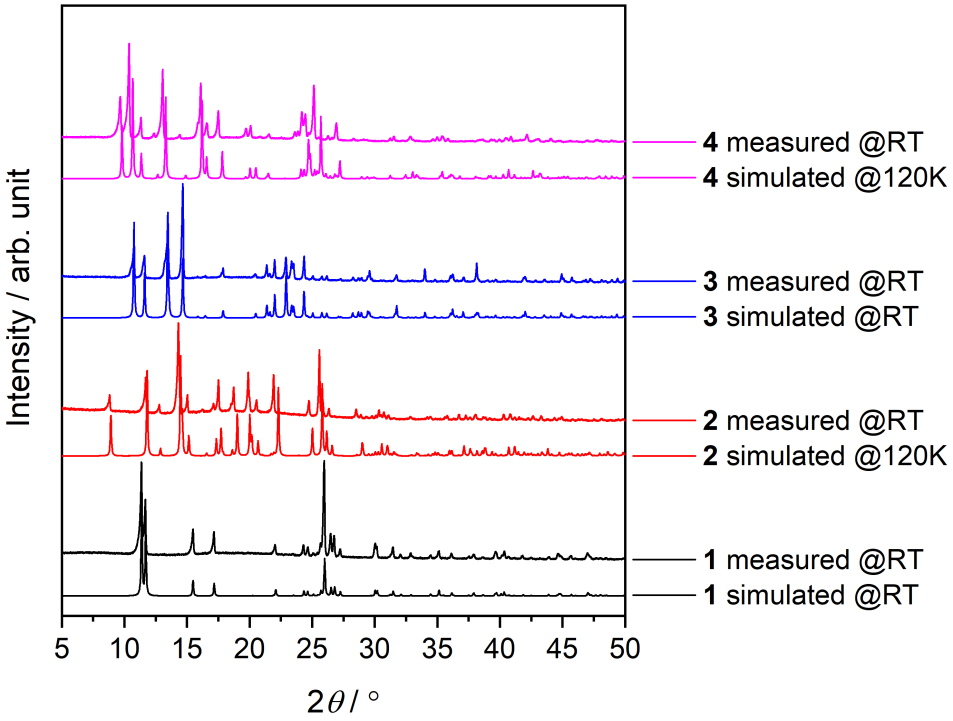

Figure S2. Normalized room-temperature (RT) powder X-ray diffractograms of **1**–**4** and the simulated powder diffractograms obtained from the single-crystal X-ray structures at the indicated temperatures.

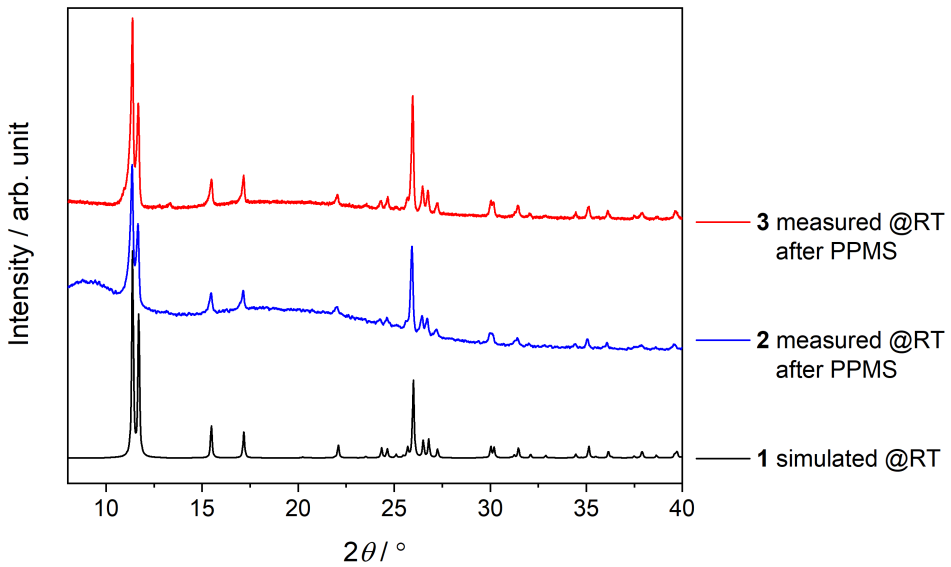

Figure S3. Normalized room-temperature (RT) powder X-ray diffractograms of **2** and **3** after the magnetization experiments shown in Fig. 3 of the main text, and the simulated powder diffractogram of **1**.

Electrochemical measurements

The electrochemical experiments were performed on a Gamry Reference 600+ Potentiostat/Galvanostat/ZRA (Gamry Instruments, Warminster, PA, USA) equipped with a 3.0 mm glassy carbon working electrode, a platinum wire auxiliary electrode, and a silver wire reference electrode. All experiments were performed at room temperature in an N_2-filled glovebox. Sample concentrations were 1.0 mM in pyridine with 0.10 M NBu_4PF_6 as the supporting electrolyte. All potentials are referenced to $Cp^*_2Fe^{0/+}$, using Cp^*_2Fe as an internal standard. The typical solvent system window with our configuration was +0.5 V for the oxidation limit and –2.25 V for the reduction limit (vs $Cp^*_2Fe^{0/+}$). Cp_2Fe (Strem) was purified according to the previously reported literature procedures. [3] Pyridine (Fisher) was dried over calcium hydride and distilled freshly. Tetrabutylammonium hexafluorophosphate (Acros) was recrystallized three times from ethanol and dried under a dynamic vacuum.[4]

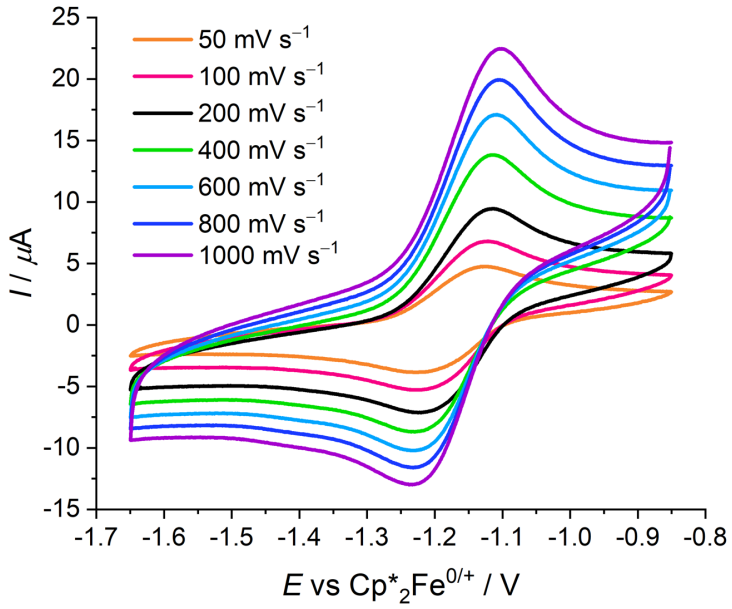

Figure S4. Cyclic voltammograms of **3** (1.0 mM) in pyridine at selected scan rates. NBu_4PF_6 (0.1 M) was used as supporting electrolyte.

Magnetic measurements

Direct current magnetization measurements were performed using the VSM options on a QuantumDesign Dynacool PPMS in the temperature range from 1.7 K to 400 K and in magnetic fields up to $\mu_0 H$ = ±9 T. The polycrystalline samples were loaded, immobilized and sealed in standard QuantumDesign powder capsules inside an argon-filled glovebox. The accurate sample masses were determined using a Mettler-Toledo WXTS3DU microbalance. The magnetization data were corrected for the intrinsic diamagnetism of both the sample and the sample capsule.

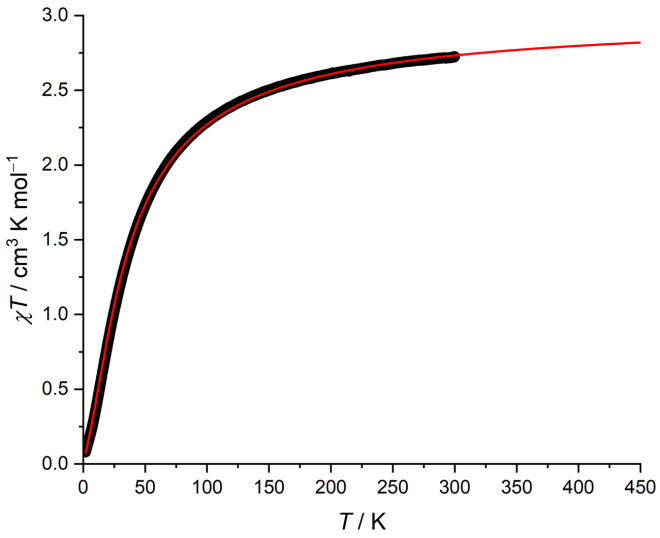

Figure S5. χT product ($\mu_0 H$ = 1.0 T) for polycrystalline **1**. The solid red line is the best fit to the classical Fisher model as described in the main text.

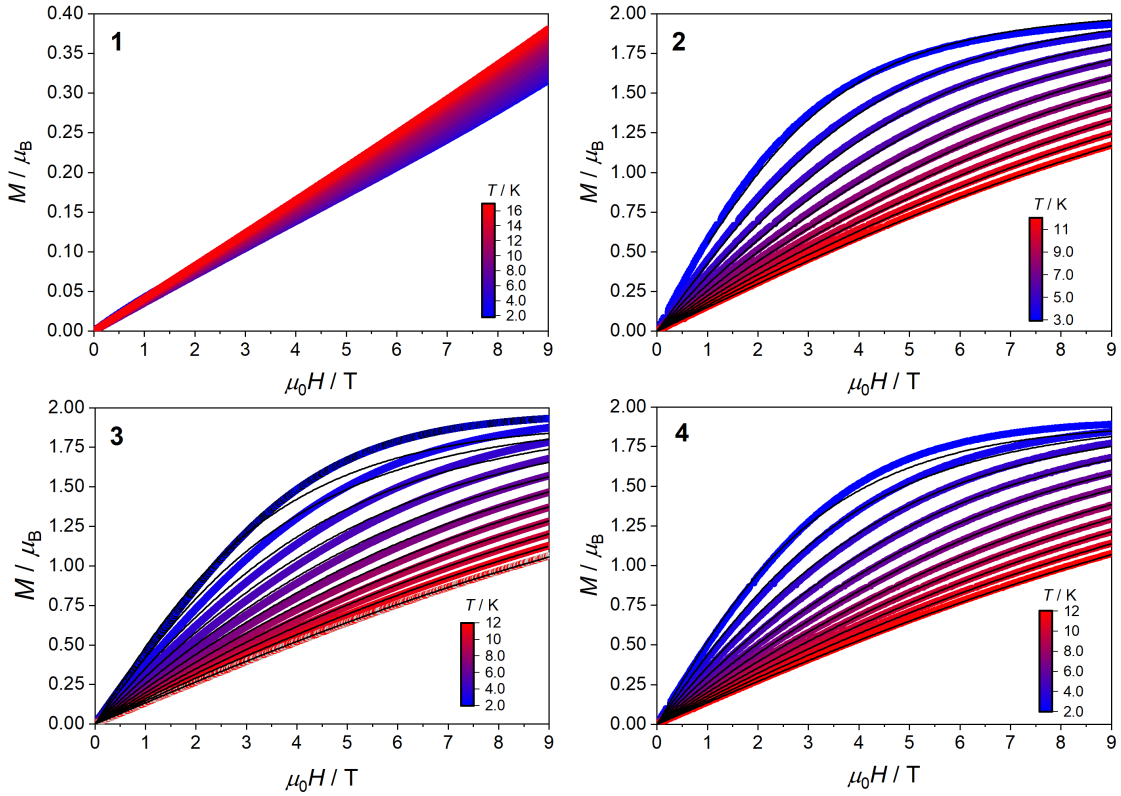

Figure S6. *M* vs $\mu_0 H$ data for polycrystalline **1**–**4** obtained at selected low temperatures. Solid black lines (**2**–**4**) are best fits using the Hamiltonian mentioned in the main text. The best fits revealed **2**: g = 2.0, $D_{S_T = 1}$ = +2.2 cm^{-1}; **3**: g = 1.9, $D_{S_T = 1}$ = +4.2 cm^{-1}; **4**: g = 1.9, $D_{S_T = 1}$ = +3.7 cm^{-1}.

Computational results

DFT calculations were performed using the ORCA program suite,[5] employing scalar relativistic effects through the 0th-order regular approximation (ZORA).[6] The experimentally determined atomic coordinates of **1** and **2** were used as input without any subsequent geometry optimization. For all calculations, the TPSSh functional[7] was combined with the scalar-relativistically recontracted (SARC) version of the triple-ζ def2-TZVP(-f) basis set[8] together with the corresponding auxiliary basis. For both systems a high-spin (HS) $S = 2$ calculation and a $S_1 = 3/2$ - $S_2 = 1/2$ broken symmetry calculation (BS(3,1)) were performed. The energy difference between the HS and BS states were employed to evaluate the exchange coupling constant, J, as defined by Yamaguchi.[9] Spin density plots and Kohn-Sham frontier orbital plots were rendered using the VMD[10] and Gabedit[11] programs, respectively.

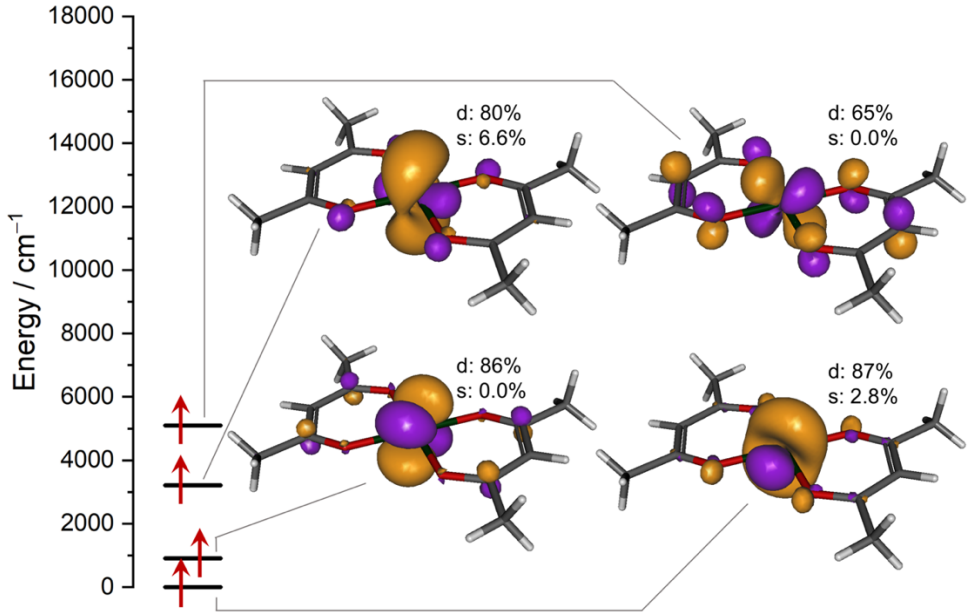

Figure S7. Qualitative frontier Kohn-Sham SOMO energy level diagram for **1** with indicated calculated relative energies and percental contribution of Cr atomic orbitals to the MOs.

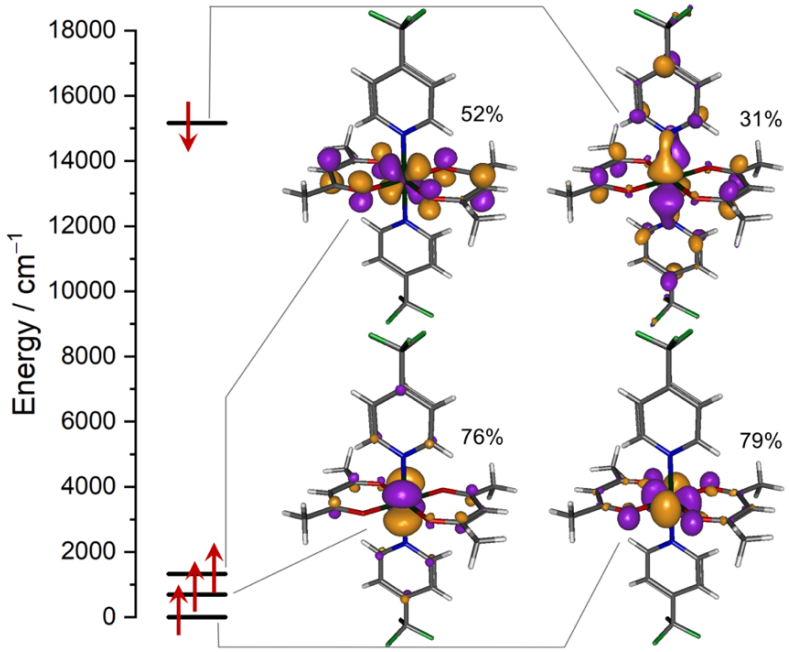

Figure S8. Qualitative frontier Kohn-Sham SOMO energy level diagram for **2** with indicated calculated relative energies and percental contribution of Cr atomic orbitals to the MOs.

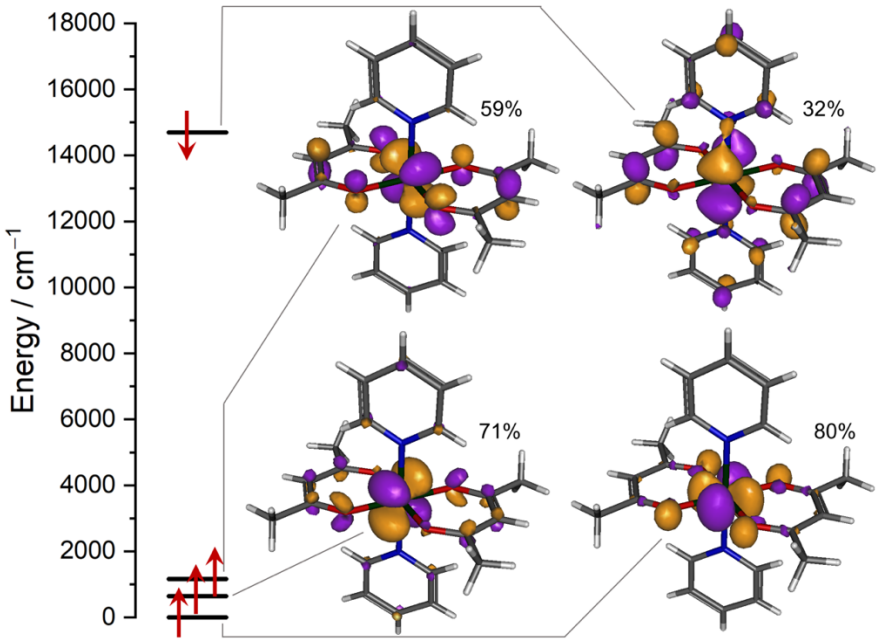

Figure S9. Qualitative frontier Kohn-Sham SOMO energy level diagram for **3** with indicated calculated relative energies and percental contribution of Cr atomic orbitals to the MOs.

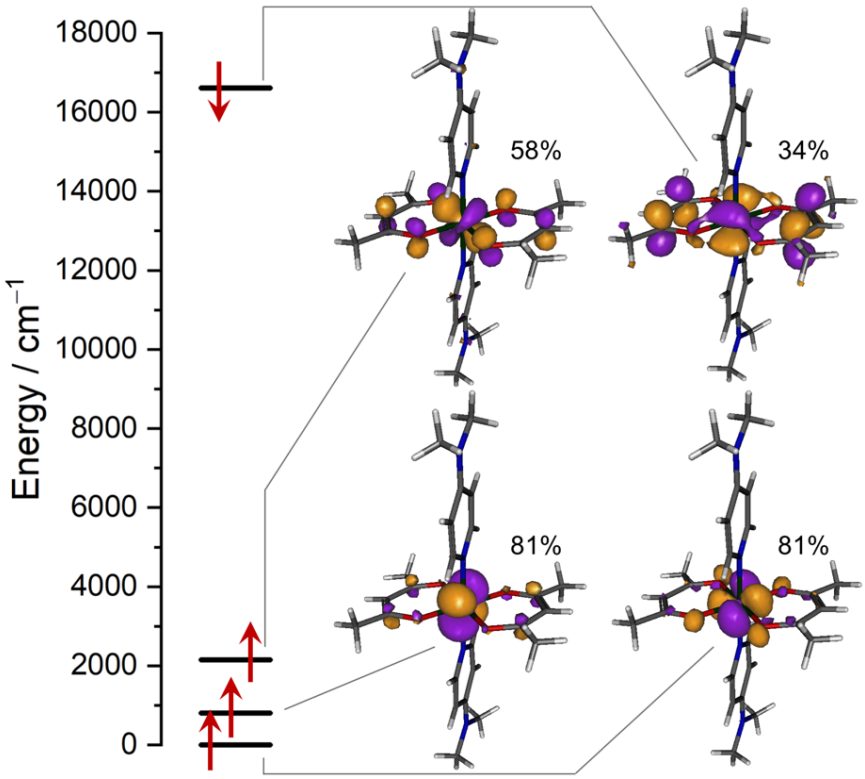

Figure S10. Qualitative frontier Kohn-Sham SOMO energy level diagram for **4** with indicated calculated relative energies and percental contribution of Cr atomic orbitals to the MOs.

References

[1] H. Dolomanov, O.V., Bourhis, L.J., Gildea, R.J, Howard, J.A.K. & Puschmann, *J. Appl. Cryst.*, 2009, **42**, 339.
[2] G. M. Sheldrick, *Acta Cryst.*, **A71**, 3–8.
[3] a) R. B. King, M. B. Bisnette, *J. Organometal. Chem.* **1967**, *8*, 287; b) A. Zahl, R. van Eldik, M. Matsumoto, T.W. Swaddle, *Inorg. Chem.* **2003**, *42*, 3718; c) J. Coddington, S. Wherland, *Inorg. Chim. Acta* **1996**, *242*, 159.
[4] R. L. Bedard, L.F. Dahl, *J. Am. Chem. Soc.* **1986**, *108*, 5933.
[5] F. Neese, *WIREs Comput. Mol. Sci.* **2018**, *8*, e1327
[6] a) E. van Lenthe, E. J. Baerends, J. G. Snijders, *J. Chem. Phys.* **1993**, *99*, 4597; b) C. J. van Wüllen, *J. Chem. Phys.* **1998**, *109*, 392.
[7] V. N. Staroverov, G. E. Scuseria, J. Tao, J. P. Perdew, *J. Chem. Phys.* **2003**, *119*, 12129.
[8] a) F. Weigend, R. Ahlrichs, *Phys. Chem. Chem. Phys.* **2005**, *7*, 3297; b) D. A. Pantazis, X.-Y. Chen, C. R. Landis, F. Neese, *J. Chem. Theory Comput.* **2008**, *4*, 908.
[9] a) K. Yamaguchi, Y. Takahara, T. Fueno, in *Applied Quantum Chemistry*; V. H. Smith, H. F. Schaefer, K. Morokuma, Eds.; D. Reidel: Boston, **1986**; p. 155; b) S. Yamanaka, T. Kawakami, H. Nagao, K. Yamaguchi, *Chem. Phys. Lett.* **1994**, *231*, 25.
[10] a) W. Humphrey, A. Dalke, K. Schulten, *J. Molec. Graphics* **1996**, 14, 33; b) Website: http://www.ks.uiuc.eu/Researcg/vmd
[11] a) A.-R. Allouche, *J. Comput. Chem.* **2010**, *32*, 174; b) Website: https://sites.google.com/site/allouchear/Home/gabedit